

Numerical Simulation of Laminar Premixed Hydrogen-Air Flame/Shock Interaction under Low-Pressure Conditions

Emilie Yhuel, Guillaume Ribert and Pascale Domingo
CORIA - CNRS, Normandie Université, INSA de Rouen Normandie
76000 Rouen, France

1 Introduction

Using Hydrogen as a fuel might seem a good solution for preventing the formation of greenhouse gases emission which is now more crucial than ever. Supposing that its production can be achieved in a eco-friendly manner (green hydrogen), an issue will still have to be dealt with: its high susceptibility to explosions if mishandled. The prediction of such a scenario by numerical simulation is therefore necessary in the prevention of disasters. In particular, numerical tools to better predict the transition scenario from deflagration to detonation are necessary [8, 15]. During the flame acceleration and transition to detonation several shocks are created and the identification of the onset of the detonation, resulting of flame/shock interactions (FSI), is the objective of the present work. To study these issues, centimetric-sized systems are preferred, whether from a numerical or experimental point of view (see [7, 21, 22]). Shock-tube configurations are the first choice to examine that problem since the FSI can occur in a well controlled environment. The flame is first established and then a shock is formed which propagates toward the flame front. The initial shape of the flame, the dimensions of the channel, the equivalence ratio of the Hydrogen/air mixture [9] are all key ingredients influencing the development of the flame inside the channel and, of course, the incident shock Mach number will be a major control parameter of the FSI. Due to the complexity of the problem, the great majority of numerical studies found in the literature have assumptions such as a unitary Lewis number or simplified chemistry. We propose here to overcome such limitations and to contribute to the description of the flame/shock interactions within the framework of the H₂/air combustion.

2 Configuration and Numerical Setup

The configuration under study corresponds to a lean hydrogen/air flame propagating from the closed end of a two-dimensional channel and facing an incoming shockwave. Two values of Mach number are considered: $M_s = 1.4$ and $M_s = 1.9$ (see Fig. 1). The half-height of the channel is $h = 35$ mm and its length, $L = 270$ mm. An adiabatic no-slip boundary conditions is applied to walls and a symmetry condition is used because gravity effects are neglected [1]. Since the mesh resolution must ensure a proper description of

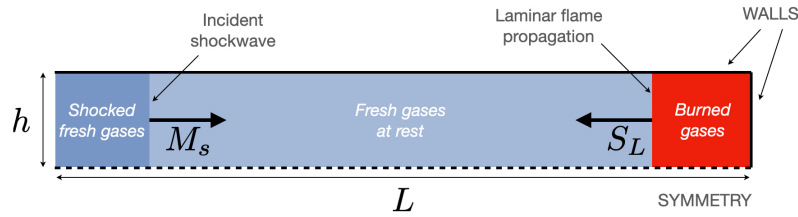


Figure 1: Sketch of the configuration under study. The H_2/air flame propagates at S_L and the incoming shockwave moves at $M_s = 1.4$ or 1.9 . $h = 35$ mm and $L = 270$ mm. In the fresh gases at rest, $P = 20$ kPa, $T = 300$ K.

the flame structure, a specific study describing the species evolution across an unstretched laminar premixed flame is proposed in section 3.1. The chemical mechanism used for the hydrogen oxydation [13] contains 9 reactive species, without nitrogen oxydes, and 23 reactions in its most recent version. In the fresh gases, the pressure (P) is set to 20 kPa, and the temperature is $T = 300$ K as initial condition.

Simulations are performed with the numerical code SiTCom-B [2, 5], which solves the conservation equations of species mass fractions, with complex molecular transport properties, momentum and total sensible energy in their fully compressible form over the structured mesh in a finite volume formulation resorting to a skew-symmetric-like scheme for the convective fluxes [4] and to a fourth-order centred scheme for the viscous and diffusive fluxes. An addition of second and fourth-order artificial dissipation terms [18–20] is used to overcome spurious oscillations [10]. Time is advanced with a fourth order Runge-Kutta scheme. Navier-Stokes characteristic boundary conditions [10, 11] are applied to describe in/outflows. Code acceleration for the calculation of chemical source terms follows the recommendations of [3].

3 Results

3.1 H_2/air Laminar Flames

The structure of an unstretched laminar premixed flames is detailed for a pressure of 20 kPa with an inlet temperature of 300 K. The results from SiTCom-B numerical code match those coming from the REGATH reference code [12], as in [3]. The flame structure obtained with REGATH is detailed in Fig. 2 for an equivalence ratio $\phi = 0.8$ with a micrometer mesh resolution in the inner flame, and over a physical domain of 10 meters. Hydrogen and oxygen decompose to mainly create H_2O and OH (Fig. 2(a)). The mass fraction of the latter exhibits a slope change (Fig. 2(b)) that is well captured by SiTComB with a coarser mesh ($\Delta x_i = 62.5 \mu\text{m}$), as shown in Fig. 2(c). Such a mesh resolution is kept for the rest of the study. Finally, the maximum temperature observed is 2144 K and the laminar flame speed is $S_L = 1.77$ m/s.

This laminar flame structure is used as initial condition (see Fig. 1) to simulate the flame propagation in the two-dimensional squared channel. The results obtained with SiTCom-B are shown in Fig. 3 through the temperature field. As already observed in the literature [9, 14, 17], the flame reorganizes in a “tulip” shape as it progresses towards the exit, on the left. Instabilities appear on the flame front that yield to an inhomogeneous temperature field in the burnt gases.

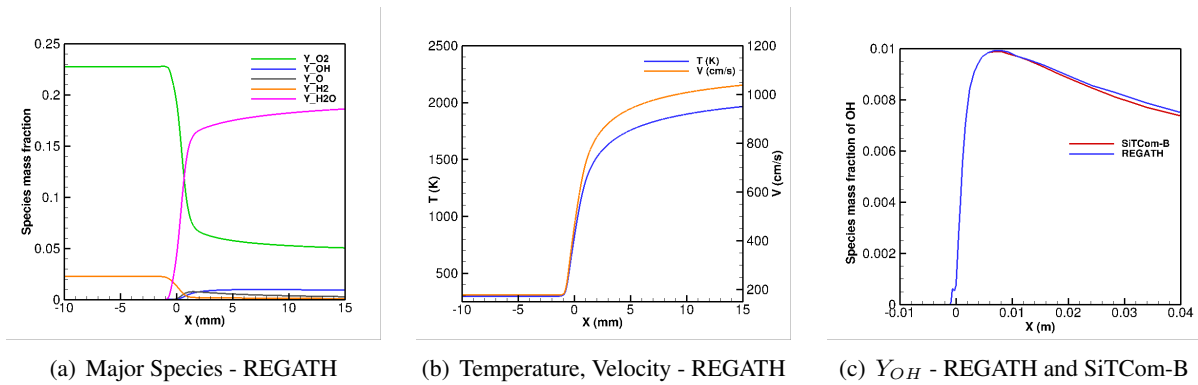


Figure 2: Structure of an H_2 /Air unstretched laminar premixed flames performed with REGATH or SiTCom-B codes. In (d), the mesh resolution is $1 \mu\text{m}$ with REGATH and $62.5 \mu\text{m}$ with SiTCom-B.

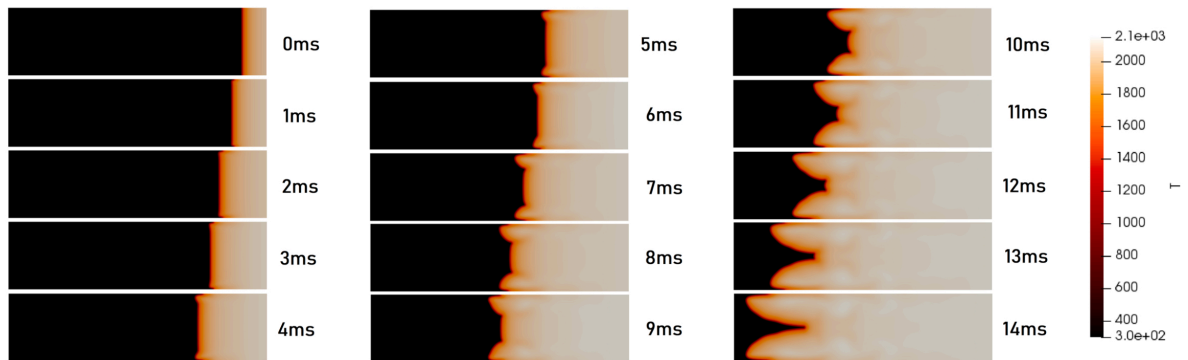


Figure 3: Temporal evolution of the H_2 /air flame propagating in a two-dimensional channel from left to right shown by the temperature field.

3.2 Flame/Shock Interaction

The flame topology observed at $t = 9 \text{ ms}$ in Fig. 3 is used as initial solution for the simulation of the flame/shock interaction. A discontinuity in pressure and temperature is created on the left part of the domain of simulation corresponding to a normal shock propagating from left to right at a Mach number of $M_s = 1.4$. A temperature of 483 K and a pressure of 80 kPa is then imposed to the shocked fresh gases. The choice of the initial flame topology is arbitrary mid-way between a strictly planar flame and a “tulip-shaped” one, in the presentation additional results will be presented to discuss the influence of the flame shape at the instant of the shock/flame first contact. In Fig. 4(a), a normal shock wave travels towards the flame with a weak expansion wave propagating towards the outlet, i.e. to the left. In Fig. 4(b), the initially normal shock wave hits the flame and an increase of temperature and Heat Release Rate (HRR) is immediately observed. The flame being curved (Fig. 4(c)), at a given instant, as it reaches the flame, the normal shock is exposed to various thermodynamic conditions along its surface. As a consequence, the shock is distorted since the portion of its surface which enters first the burnt gases is accelerated. Close to the walls, the flame surface is then flattened as it is pushed toward the back wall by the shock. It is readily observed that the pressure gradient decreases in the burnt gases, while the HRR increases as the shock passes through the

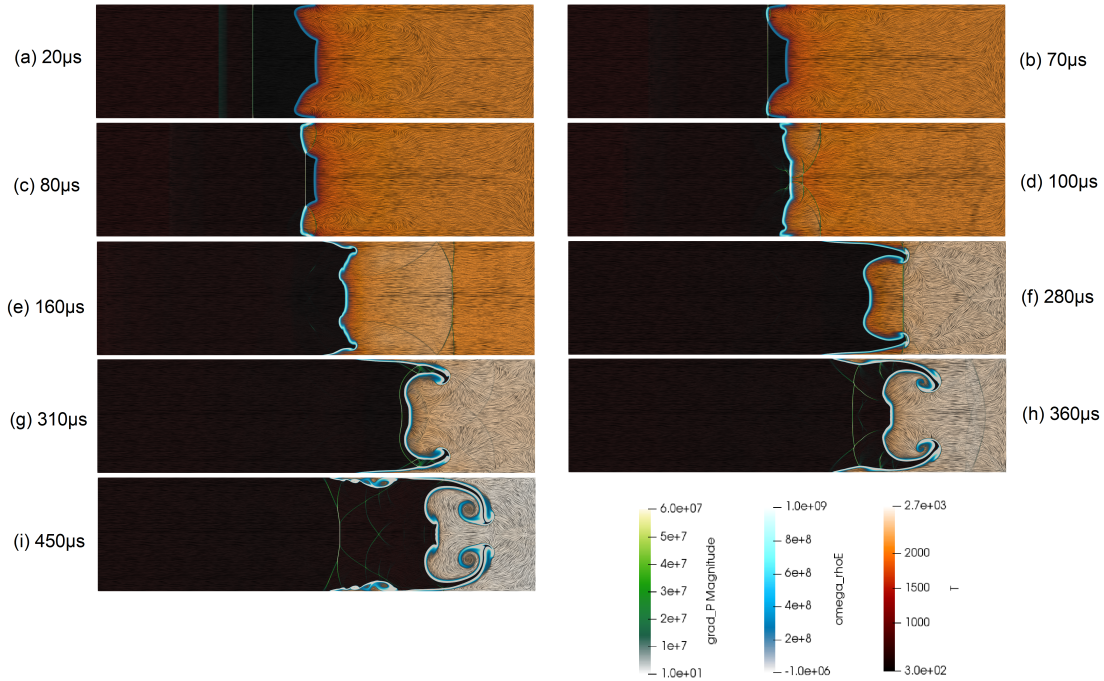


Figure 4: Temporal evolution of a shock coming from the left interacting with a flame initiated from the right. In green, pressure gradient (∇P) to highlight the arrangements of the shocks; in blue, heat release rate ($\dot{\omega}_{\rho E}$) to depict the flame front; in red, temperature (T) with streamlines.

flame front (Fig. 5(a)). Once the shock has entirely crossed the flame (Fig. 4(d)), the whole flame front appears flattened and the flame changes its direction of propagation being pushed toward the back wall. Instabilities begin to appear near the top and bottom walls. The reflected shock waves give rise to triple points which propagate in the burnt gases. In Fig. 4(e), the shock structure and the flame progress towards the back wall. The flame begins to stretch following the arrangement of the transverse waves, and because of the high speed behind the shock wave which contrasts with the low speed in the boundary layers. The shock is reflected on the back wall between 200 and 210 μs and becomes close again to a normal shock. Then it crosses the flame front for the second time going now from burnt gases to fresh gases. The temperature in the burnt gases rises again after the reflection of the shock. During this second FSI (Fig. 4(f)), the HRR increases vigorously at the flame front, as shown in Fig. 5(a), with the mean HRR conditioned to the progress variable $c = Y_{H_2O}/Y_{H_2O}^{eq} = 0.5$, $HRR|_{c=0.5}$, with $Y_{H_2O}^{eq}$ the equilibrium value of the 1D flame used for initialisation, and HRR_0 the $HRR|_{c=0.5}$ of the 1D flame.

Reflected pressure waves are seen behind the reflected shock wave, which from being nearly flat is starting to bend. The flame keeps on moving towards the back wall, giving rise to vortices resulting from Richtmyer-Meshkov instabilities (Fig. 4(g)). Several wave reflections are observed behind the shock and the pressure gradient increases again as it passes through the fresh gases (Fig. 4(h)). At 450 μs (Fig. 4(i)), the shockwave continues to propagate towards the exit, while instabilities develop with the formation of triple points due to the reflections of waves on the walls and in the instabilities. From 360 μs , the flame begins to display two very different behaviours: (1) the central part of the flame continues to be pushed toward the back wall and (2) the flame in the vicinity of the top and bottom walls benefits from a zone of low velocity and propagates inside the boundary layers. At 450 μs , the flame front becomes discontinuous and a separation occurs

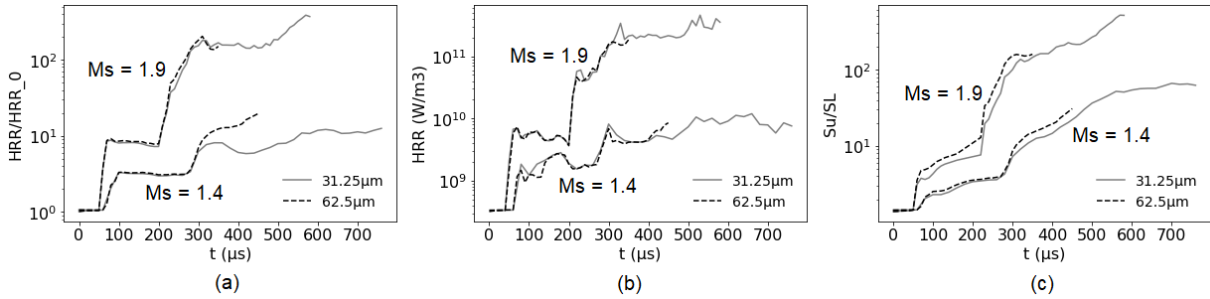


Figure 5: Temporal evolution of (a) Mean Heat Release Rate conditioned to $c = 0.5$, (b) Maximum Heat Release Rate in the domain, (c) Burning flame velocity.

between the two flame regions which are now driven by different mechanism. Kelvin-Helmoltz instabilities have begun to develop in the boundary layers. At the end of the second shock-flame, temperature has increased considerably from 2100 K to 2700 K and the maximum HRR has nearly doubled (Fig. 5(b)). The burning flame velocity S_u has also increased during the two FSI, as shown in Fig. 5(c), where $S_u = \iint_S \dot{\omega}_{Y_{H_2O}} dS / [(Y_{H_2O}^b - Y_{H_2O}^u) \rho_u h]$.

The impact of mesh resolution has been investigated (see Fig. 5), increasing the resolution by a factor 2. The impact of the mesh resolution is barely visible for the two successive FSI. However, a significant difference appears when the boundary layer develops and the separation occurs.

The simulation has also been performed with an incident shock Mach number 1.9. The stages described for Mach 1.4 are recovered with a shift in time apparition. However, the increase in heat release and burning flame velocity are more than doubled compared to Mach 1.4 ((Fig. 5). Further increasing the incident Mach number shock is expected to lead to detonation.

4 Conclusion

Within the framework of the use of hydrogen as an energy vector, a study relating to the numerical simulation of the propagation of a laminar flame in a channel and interacting with a normal shockwave is proposed. Since the laminar flame can not be flat because of the non-slip wall condition, the initial plane shock bends at the crossing of the flame front. The high speed of the shock pushes the flame towards the back wall, and the reflected wave splits the flame into two parts, one progressing again toward the fresh gases make using of the velocity deficit in the top and bottom boundary layers and the other reorganising itself at the back of the channel displaying significant Richtmyer-Meshkov instabilities. In such situation in term of Mach number and mixture equivalence ratio, no detonation appears. In the final presentation, the influence of the initial flame front shape and of more realistic isothermal boundary conditions will be explored.

5 Acknowledgments

The first author is founded by the Agence Nationale de la Recherche in the framework of the project ANR-20-CE05-0014 - PHYSSA: Propagation of HYdrogen flameS for Safety Applications. This work was granted access to the HPC resources of CRIANN (Centre Régional Informatique et d'Applications Numériques de Normandie).

References

- [1] Bioche K., Pieyre A., Ribert G., Richecoeur F., Vervisch L. (2019). The role of gravity in the asymmetry of flames in narrow combustion chambers, *Combust. Flame* 203: 238–246.
- [2] Bouheraoua L., Domingo P., Ribert G. (2017). Large-eddy simulation of a supersonic lifted jet flame: Analysis of the turbulent flame base. *Combust. Flame* 179: 199–218.
- [3] Duboc B., Ribert G., Domingo P. (2019). Hybrid transported-tabulated chemistry for partially premixed combustion, *Computers Fluids* 179: 206–227.
- [4] Ducros F., Ferrand V., Nicoud F., Weber C., Darracq D., Gacherieu C., Poinot T. (1999). Large-eddy simulation of the shock/turbulence interaction. *J. Comput. Phys.* 152: 517–549.
- [5] Guven U., Ribert G. (2018). Large-eddy simulation of supersonic hydrogen/oxygen combustion: application to rocketlike igniter. *J. Propul. Power* 34: 291–307.
- [6] Jiang H., Dong G., Xiao C., Li B. (2016). A parametrization of the Richtmyer-Meshkov instability on a premixed flame interface induced by the successive passages of shock waves. *Combust. Flame* 169: 229–241.
- [7] Li X., Xiao H., Duan Q., Sun J. (2021). Numerical study of premixed flame dynamics in a closed tube : Effect of wall boundary condition. *Proc. Combust. Inst.* 38: 2075–2082.
- [8] Oran E. (2015). Understanding explosions - From catastrophic accidents to creation of the universe. *Proc. Combust. Inst.* 35(1): 1–35.
- [9] Oran E., Xiao H., Houim R. (2015). Formation and evolution of distorted tulip flames. *Combust. Flame*, 162: 4084–4101.
- [10] Petit X., Ribert G., Lartigue G., Domingo P. (2013). Large-eddy simulation of supercritical fluid injection. *J. Supercritical Fluids*. 84: 61–73.
- [11] Poinot T., Lele S. (1992). Boundary conditions for direct simulations of compressible viscous flows. *J. Comput. Phys.* 101: 104–129.
- [12] Ribert G., Petit X., Domingo P. (2017). High-pressure methane-oxygen flames. Analysis of sub-grid scale contributions in filtered equations of state, *J. Supercritical Fluids* 121: 78–88.
- [13] <https://web.eng.ucsd.edu/mae/groups/combustion/mechanism.html>
- [14] Sawyer R., Dunn-Rankin D., Barr P. (1986). Numerical and experimental study of “tulip” flame formation in a closed vessel. *Symp. Int. Combust.* 21: 1291–1301.
- [15] Shepherd J.E. (2009). Detonation in Gases. *Proc. Combust. Inst.* 32(1): 83–98.
- [16] Shen J., He X. (2015). A comparative study on premixed hydrogen-air and propane-air flame propagations with tulip distortion in a closed duct. *Fuel*, 161: 248–253.
- [17] Sun J., Molkov V., Xiao H., Makarov D. (2012). Experimental and numerical investigation of premixed flame propagation with distorted tulip shape in a closed duct. *Combust. Flame*, 159: 1523–1538.
- [18] Swanson R., Turkel E. (1992). On central-difference and upwind schemes. *J. Comput. Phys.* 101: 292–306.
- [19] Swanson R., Radespiel R., Turkel E. (1998). On some numerical dissipation schemes. *J. Comput. Phys.* 147: 518–544.
- [20] Tatsumi S., Martinelli L., Jameson A. (1995). Flux-limited schemes for the compressible Navier-Stokes equations. *AIAA J.* 33: 252–261.
- [21] Yang H., Radulescu M. (2021). Enhanced DDT mechanism from shock-flame interactions in thin channels. *Proc. Combust. Inst.* (3)38: 3481–3495.
- [22] Yang H., Radulescu M. (2021). Dynamics of cellular flame deformation after a head-on interaction with a shock wave: reactive Richtmyer-Meshkov instability. *Journal of Fluids Mechanics* (923).